Mineralogical Magazine (2022), **86**, 767–776
doi:10.1180/mgm.2022.54

CAMBRIDGE UNIVERSITY PRESS

Article

Uvite, $CaMg_3(Al_5Mg)(Si_6O_{18})(BO_3)_3(OH)_3(OH)$, a new, but long-anticipated mineral species of the tourmaline supergroup from San Piero in Campo, Elba Island, Italy

Ferdinando Bosi[1]*, Cristian Biagioni[2], Federico Pezzotta[3], Henrik Skogby[4], Ulf Hålenius[4], Jan Cempírek[5], Frank C. Hawthorne[6], Aaron J. Lussier[6,7], Yassir A. Abdu[6,8], Maxwell C. Day[6], Mostafa Fayek[6], Christine M. Clark[9], Joel D. Grice[7] and Darrell J. Henry[10]

[1]Dipartimento di Scienze della Terra, Sapienza Università di Roma, Piazzale Aldo Moro 5, I–00185, Rome, Italy; [2]Dipartimento di Scienze della Terra, Università di Pisa, Via Santa Maria 53, I–56126 Pisa, Italy; [3]Natural History Museum, Corso Venezia 55, 20121 Milan, Italy; [4]Department of Geosciences, Swedish Museum of Natural History, P.O. Box 50 007, SE–104 05 Stockholm, Sweden; [5]Department of Geological Sciences, Faculty of Science, Masaryk University, Kotlářská 2, 611 37, Brno, Czech Republic; [6]Department of Earth Sciences, University of Manitoba, Winnipeg, Manitoba R3T 2N2, Canada; [7]Research Division, Canadian Museum of Nature, PO Box 3443, Station D, Ottawa, Ontario, Canada K1P 6P4; [8]Department of Applied Physics and Astronomy, University of Sharjah, 27272, Sharjah, United Arab Emirates; [9]Department of Geography and Geology, Eastern Michigan University, Ypsilanti, Michigan 48197, USA; and [10]Department of Geology and Geophysics, Louisiana State University, Baton Rouge, Louisiana 70803, USA

Abstract

Uvite, $CaMg_3(Al_5Mg)(Si_6O_{18})(BO_3)_3(OH)_3(OH)$, is a new mineral of the tourmaline supergroup. It occurs in the Facciatoia quarry, San Piero in Campo, Elba Island, Italy (42°45′04.55″N, 10°12′50.89″E) at the centre of a narrow (2–3 cm wide) vein composed of aggregates of dark brown to black tourmaline, penetrating (magnesite + dolomite)-rich hydrothermally altered metaserpentinite. Crystals are euhedral and up to 1 cm in size, brown with a vitreous lustre, conchoidal fracture and grey streak. Uvite has a Mohs hardness of ~7½, a calculated density of 3.115 g/cm^3 and is uniaxial (–). Uvite has trigonal symmetry, space group $R3m$, $a = 15.9519(10)$ Å, $c = 7.2222(5)$ Å, $V = 1597.3(1)$ Å^3 and $Z = 3$. The crystal structure was refined to $R_1 = 1.77\%$ using 1666 unique reflections collected with Mo$K\alpha$ X-rays. Crystal-chemical analysis resulted in the empirical crystal-chemical formula $^{X}(Ca_{0.61}Na_{0.35}\square_{0.04})_{\Sigma 1.00}{}^{Y}(Mg_{1.50}Fe^{2+}_{0.47}Al_{0.71}Fe^{3+}_{0.14}Ti_{0.18})_{\Sigma 3.00}{}^{Z}(Al_{4.54}Fe^{3+}_{0.18}V^{3+}_{0.02}Mg_{1.27})_{\Sigma 6.00}{}^{T}[(Si_{5.90}Al_{0.10})_{\Sigma 6.00}O_{18}](BO_3)_3{}^{O(3)}(OH)_3{}^{O(1)}[(OH)_{0.55}F_{0.05}O_{0.40}]_{\Sigma 1.00}$

which recast in its ordered form for classification purposes is:

$$^{X}(Ca_{0.61}Na_{0.35}\square_{0.04})_{\Sigma 1.00}{}^{Y}(Mg_{2.35}Fe^{2+}_{0.47}Ti_{0.18})_{\Sigma 3.00}$$
$$^{Z}(Al_{5.25}Fe^{3+}_{0.32}V^{3+}_{0.02}Mg_{0.42})_{\Sigma 6.00}{}^{T}[(Si_{5.90}Al_{0.10})_{\Sigma 6.00}O_{18}](BO_3)_3{}^{V}(OH)_3{}^{W}[(OH)_{0.55}F_{0.05}O_{0.40}]_{\Sigma 1.00}$$

Uvite is a hydroxy-species belonging to the calcic-group of the tourmaline supergroup. The closest end-member compositions of valid tourmaline species are fluor-uvite and feruvite, to which uvite is related by the substitutions $^{W}(OH)^- \leftrightarrow {}^{W}F^-$ and $^{Y}Mg^{2+} \leftrightarrow {}^{Y}Fe^{2+}$, respectively. The occurrence of a solid-solution between uvite and magnesio-lucchesiite, according to the substitution $^{Z}Mg^{2+} + {}^{W}(OH)^- \leftrightarrow {}^{Z}Al^{3+} + {}^{W}O^{2-}$, is supported by experimental data. The new mineral was approved by the IMA–CNMNC (IMA 2019-113). Uvite from Facciatoia formed by the reaction between B-rich fluids, released during the crystallisation process of LCT pegmatites, and the surrounding metaserpentinites, altered by contact metamorphism in the aureole of the Miocene Mt. Capanne monzogranitic pluton.

Keywords: uvite, new mineral species, tourmaline, crystal-structure refinement, electron microprobe, Mössbauer spectroscopy, infrared spectroscopy, optical absorption spectroscopy

(Received 15 February 2022; accepted 20 May 2022; Accepted Manuscript published online: 31 May 2022; Associate Editor: David Hibbs)

Introduction

Tourmalines are complex borosilicates that have been studied extensively in terms of their crystal structure and crystal chemistry (e.g. Foit, 1989; Hawthorne, 1996; Hawthorne and Henry, 1999; Ertl *et al.*, 2002; Novák *et al.*, 2004; Bosi, 2013, 2018; Henry and Dutrow, 2011; Cempírek *et al.*, 2013; Bačík and Fridrichová, 2021). In accordance with Henry *et al.* (2011), the

*Author for correspondence: Ferdinando Bosi, Email: ferdinando.bosi@uniroma1.it
Cite this article: Bosi F., Biagioni C., Pezzotta F., Skogby H., Hålenius U., Cempírek J., Hawthorne F.C., Lussier A.J., Abdu Y.A., Day M.C., Fayek M., Clark C.M., Grice J.D. and Henry D.J. (2022) Uvite, $CaMg_3(Al_5Mg)(Si_6O_{18})(BO_3)_3(OH)_3(OH)$, a new, but long-anticipated mineral species of the tourmaline supergroup from San Piero in Campo, Elba Island, Italy. *Mineralogical Magazine* **86**, 767–776. https://doi.org/10.1180/mgm.2022.54

general chemical formula of tourmaline is written as: $XY_3Z_6T_6O_{18}(BO_3)_3V_3W$, where $X = Na^+$, K^+, Ca^{2+}, □ (= vacancy); $Y = Al^{3+}$, Fe^{3+}, Cr^{3+}, V^{3+}, Mg^{2+}, Fe^{2+}, Mn^{2+}, Li^+; $Z = Al^{3+}$, Fe^{3+}, Cr^{3+}, V^{3+}, Mg^{2+}, Fe^{2+}; $T = Si^{4+}$, Al^{3+}, B^{3+}; $B = B^{3+}$; $V = (OH)^-$, O^{2-}; and $W = (OH)^-$, F^-, O^{2-}. Note that the letters X, Y, T, Z and B represent groups of cations at the $^{[9]}X$, $^{[6]}Y$, $^{[6]}Z$, $^{[4]}T$ and $^{[3]}B$ crystallographic sites (designated by italicised letters). The letters V and W in the formula represent groups of anions accommodated at the [3]-coordinated O(3) and O(1) crystallographic sites, respectively. The dominance of specific ions at one or more sites of the structure gives rise to numerous distinct mineral species.

A formal description of the new tourmaline species uvite is presented here. Uvite is a common mineral name in the tourmaline literature and refers to the province of Uva (Sri Lanka) as the type locality for the formerly supposed occurrence of this mineral (Kunitz, 1929). However, the tourmaline from the Uva locality should actually correspond to a fluor-species (Dunn *et al.*, 1977). In accord with the tourmaline nomenclature scheme, the root name of fluor-uvite (Henry *et al.*, 2011) requires that the name uvite should be given to the hydroxy analogue. The approval of this new species has been beset by difficulties. Uvite was approved by the International Mineralogical Association's Commission on New Minerals, Nomenclature and Classification (IMA–CNMNC) as a valid mineral species with the proposal no. 2000-030a (Clark *et al.*, 2010), but the complete description has never been published. This proposal was subsequently withdrawn as additional analytical work done by the authors of proposal 2000-30a showed this material to be a potentially new oxy-tourmaline (Hålenius *et al.*, 2018). In July 2019, another proposal (no. 2019-004) was rejected. Finally, uvite has been approved by the IMA–CNMNC with proposal no. 2019-113 (Bosi *et al.*, 2020) using a specimen collected at Facciatoia, at the eastern limit of the village of San Piero in Campo, Elba Island, in an abandoned magnesite quarry in 2019 by the mineral collector Michele Degl'Innocenti. Holotype material is deposited in the collections of the Natural History Museum of Milano, Italy, catalogue number M38848, and the Museo di Storia Naturale, University of Pisa, catalogue number 19911.

Occurrence

The holotype specimen was collected from a narrow vein of aggregates of dark brown-to-black tourmaline, penetrating hydrothermally altered metaserpentinite rich in magnesite and dolomite, in the abandoned Facciatoia quarry, east of the village of San Piero in Campo, Elba Island, Livorno, Tuscany, Italy (42° 45′04.55″N, 10°12′50.89″E). Facciatoia is a classic mineralogical locality, in which several narrow LCT pegmatites rich in multicoloured and pink elbaite crystals were found in the past (today the locality is exhausted; Pezzotta, 2021); the pegmatites crosscut a lens of porphyritic monzogranite and the surrounding hydrothermally altered metaserpentinites.

In San Piero in Campo, tourmaline-rich veins typically cross-cut metaserpentinites around miarolitic tourmaline-bearing pegmatites in the metamorphic aureole of the Monte Capanne intrusion. These veins are up to 2 or 3 cm wide and can be up to a few metres long. They are entirely composed of tourmaline-supergroup minerals (uvite and magnesio-lucchesiite), and locally form small cavities in which tourmaline occurs as blackish sharp and lustrous short prisms, up to 1 cm long and 5 mm in diameter.

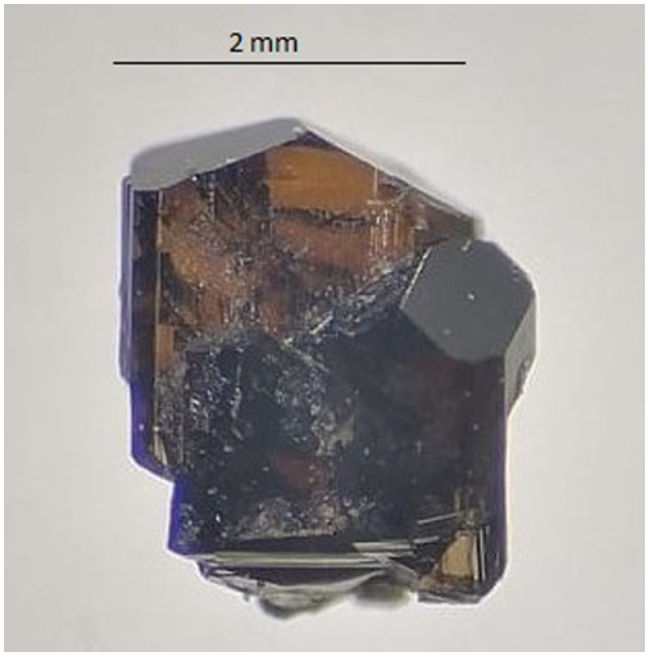

Fig. 1. Photo of the holotype fragment (#19911) of uvite in transmitted light.

Appearance, physical and optical properties

Uvite occurs as massive vein-filling subhedral grains and rare euhedral crystals up to 1 cm in size and is brown with a vitreous lustre (Fig. 1). The morphology consists of $\{10\bar{1}0\}$ and $\{11\bar{2}0\}$ prisms terminated by $\{10\bar{1}1\}$ and $\{10\bar{1}\bar{1}\}$ pyramidal faces. Prism faces are striated parallel to the **c** axis. It has a grey streak and shows no fluorescence, has a Mohs hardness of ~7½ (estimated by analogy with magnesio-lucchesiite; Scribner *et al.*, 2021) and is brittle with a conchoidal fracture. The calculated density, based on the empirical formula and unit-cell volume refined from single-crystal X-ray diffraction (XRD) data, is 3.115 g/cm^3. In thin section, uvite is transparent; in transmitted light, it is pleochroic, O = greenish brown, E = pale yellow, with O > E. Uvite is uniaxial (–) with refractive indices $\omega = 1.660(5)$ and $\varepsilon = 1.640(5)$ measured by the immersion method using white light from a tungsten source. The mean index of refraction, density, and chemical composition resulted in an excellent compatibility index ($1 - Kp/Kc = 0.021$) (Mandarino, 1981).

Analytical methods and results

Microprobe analysis

Electron microprobe analysis was done using a wavelength-dispersive spectrometer (WDS mode) with a Cameca SX50 instrument at the 'Istituto di Geologia Ambientale e Geoingegneria, CNR (Rome, Italy)', operating at an accelerating potential of 15 kV, a sample current of 15 nA and 10 μm beam diameter. The following standards, X-ray *K*α lines and analyser crystals were used: wollastonite (Si and Ca; PET), magnetite (Fe; LIF), rutile (Ti; PET), corundum (Al; TAP), vanadinite (V; PET), fluorophlogopite (F; TAP), periclase (Mg; TAP), jadeite (Na; TAP), orthoclase (K; PET), sphalerite (Zn; LIF), chromium oxide (Cr; PET), and metallic Mn (Mn; LIF). The PAP routine was applied (Pouchou and Pichoir, 1991). Table 1 gives mean

https://doi.org/10.1180/mgm.2022.54 Published online by Cambridge University Press

Table 1. Electron microprobe data (WDS mode) and atoms per formula unit (apfu) normalised to 31 anions for uvite.

Wt.%	Mean (15 spots)	Range	S.D.	apfu
SiO_2	35.45	34.69–36.69	0.42	5.895
TiO_2	1.40	1.03–1.84	0.23	0.176
B_2O_3[a]	10.45			3.000
Al_2O_3	27.30	26.06–27.98	0.51	5.350
V_2O_3	0.12	0.07–0.17	0.03	0.015
FeO_{tot}	5.68	4.11–6.36	0.67	—
MgO	11.19	10.55–12.13	0.51	2.774
CaO	3.43	2.96–3.89	0.27	0.610
Na_2O	1.10	0.82–1.32	0.14	0.354
F	0.11	0.00–0.17	0.06	0.055
H_2O[a]	3.30			3.547
O = F	−0.04			
Fe_2O_3[b]	2.52			0.316
FeO[b]	3.41			0.474
Total	99.63			

[a]Calculated by stoichiometry, (Y + Z+T) = 15.00 apfu.
[b]Determined by Mössbauer spectroscopy
S.D. – standard deviation

values of 15 spot analyses. Chromium, Mn, Zn and K were below detection limits (<0.03 wt.%).

Mössbauer spectroscopy

Mössbauer spectroscopy (MS) was used to determine the $Fe^{3+}/\Sigma Fe$ ratio of the sample, using a conventional spectrometer system operated in constant acceleration mode (Swedish Museum of Natural History, Stockholm, Sweden). The absorber was prepared from 40 mg of ground sample mixed with an acrylic resin which was pressed to a 12-mm diameter disc under mild heating (<150°C). Data were collected over 1024 channels in the velocity range −4.2 to +4.2 mm/s using a ^{57}Co rhodium matrix standard source of 50 mCi nominal activity and were calibrated and folded against the spectrum of an α-Fe foil. The spectrum (Fig. 2) was fit using the software *MossA* (Prescher *et al.*, 2012) with three doublets assigned to Fe^{2+} and one doublet assigned to Fe^{3+}, resulting in an $Fe^{3+}/\Sigma Fe$ ratio of 0.40, assuming similar recoil-free fractions for Fe^{2+} and Fe^{3+} (Table 2).

Single-crystal infrared spectroscopy

Polarised Fourier-transform infrared (FTIR) absorption spectra were measured on a 39 μm thick doubly polished single-crystal section oriented parallel to the **c**-axis. A Bruker Vertex 70 spectrometer attached to a Hyperion 2000 microscope was used to collect spectra in the range 2000–13000 cm^{-1} at a resolution of 4 cm^{-1} (Swedish Museum of Natural History, Stockholm, Sweden). Spectra recorded in polarised mode parallel to the crystallographic **c**-axis show a very intense band at ~3570 cm^{-1}, which is off-scale due to excessive absorption, and three less-intense bands at 3666, 3728 and 3764 cm^{-1} (Fig. 3). A shoulder occurs around 3623 cm^{-1}. Spectra obtained perpendicular to the **c**-axis show considerably weaker bands at 3577 and 3623 cm^{-1}, which may be the bands responsible for the very strong absorption in the opposite polarisation direction.

Bands above about 3600–3650 cm^{-1} are usually due to (OH) at the O(1) site (≡ W) (e.g. Gonzalez-Carreño *et al.*, 1988; Bosi *et al.*, 2015a). Based on the empirical crystal-chemical formula (see below) and the studies of Watenphul *et al.* (2016) and Bosi *et al.* (2018), the main FTIR bands at ~3577 cm^{-1} are probably

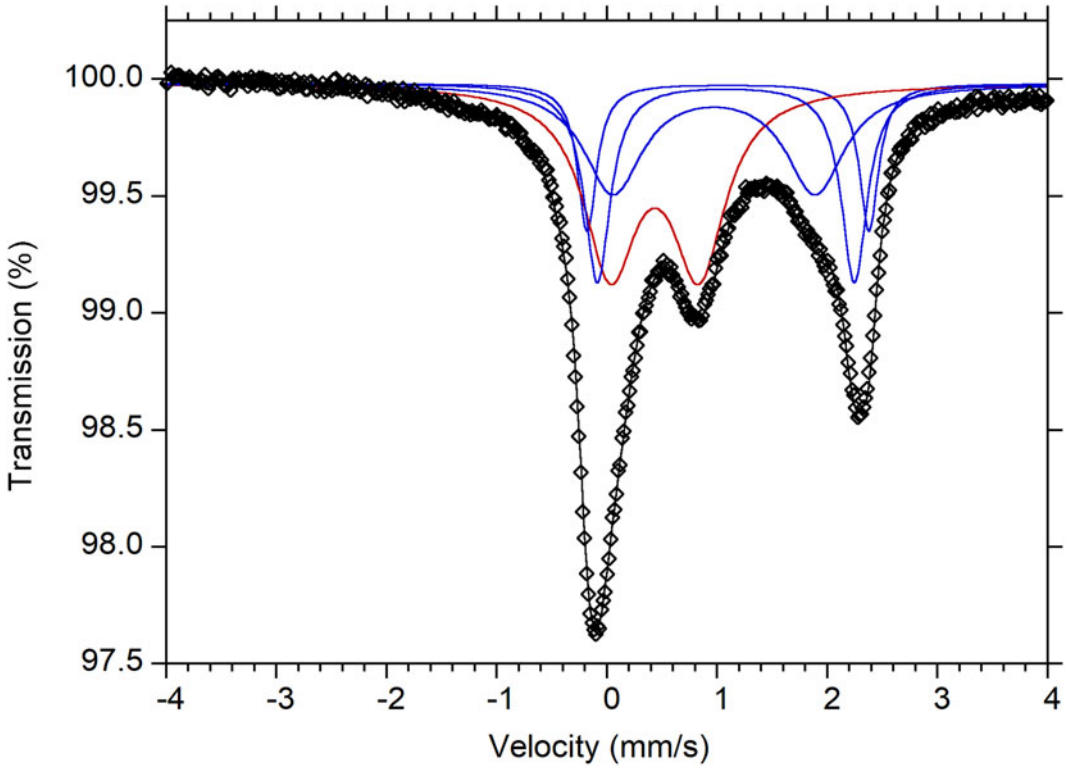

Fig. 2. Mössbauer spectrum of uvite. Fitted absorption doublets assigned to Fe^{2+} and Fe^{3+} are indicated in blue and red, respectively. Diamonds denote the measured spectrum, and the black curve represents summed fitted spectra.

https://doi.org/10.1180/mgm.2022.54 Published online by Cambridge University Press

Table 2. Mössbauer parameters for uvite obtained at room-temperature.*

δ (mm/s)	ΔE_Q (mm/s)	FWHM (mm/s)	*A*(%)	Assignment
1.08	2.33	0.28	21.5	$^{[6]}Fe^{2+}$
1.10	2.56	0.21	11.7	$^{[6]}Fe^{2+}$
0.97	1.84	0.64	26.6	$^{[6]}Fe^{2+}$
0.43	0.81	0.59	40.2	$^{[6]}Fe^{3+}$

*δ = centroid shift, ΔE_Q = quadrupole splitting, FWHM = full width at half-maximum, *A* = relative area.

caused by the atomic arrangements {2[(Fe,Mg)AlAl]–(AlAlAl)}–$^{O(3)}(OH)_3$, whereas we prefer to ascribe the band at ~3623 to the arrangements 3[(Fe,Mg)AlAl]–$^{O(3)}(OH)_3$ rather than to ^{Y}[(Fe,Mg)AlAl]–$^{O(1)}$(OH)–^{X}(□) because the ^{X}□ content is too low. The latter arrangement is more likely to be related to the band at ~3666 cm^{-1} in the atomic arrangement ^{Y}(MgMgAl)–$^{O(1)}$(OH)–^{X}(□). In this regard, note that the bands between ~3650–3700 cm^{-1} are associated with ^{X}□, whereas those above 3700 cm^{-1} are associated with ^{X}(Na,Ca) (e.g. Gonzalez-Carreño *et al.*, 1988; Berryman *et al.*, 2016; Watenphul *et al.*, 2016). Consequently, bands at ~3728 and ~3764 cm^{-1} may be due to the arrangements ^{Y}(FeFeAl)–$^{O(1)}$(OH)–^{X}(Na) and ^{Y}(MgMgMg)–$^{O(1)}$(OH)–^{X}(Na,Ca), respectively.

Optical absorption spectroscopy (OAS)

Polarised optical absorption spectra of uvite (Fig. 4) were acquired at the Natural History Museum of Stockholm, Sweden. Data were collected at room temperature on the same polished crystal that was used for FTIR measurements. An AVASPEC-ULS2048X16 spectrometer, connected via a 400 μm UV fibre cable to a Zeiss Axiotron UV-microscope, was used. A 75 W Xenon arc lamp was used as a light source and Zeiss Ultrafluar 10× lenses served as objective and condenser. A UV-quality Glan-Thompson prism, with a working range from 40000 to 3704 cm^{-1}, was used as the polariser.

The recorded spectra show broad and strongly polarised (O > E) absorption bands at 22000, 14250 and 8790 cm^{-1} (Fig. 4). In agreement with previous optical studies of tourmaline (e.g. Mattson and Rossman, 1987), the bands at 14250 and 8790 cm^{-1} are assigned to Fe^{3+}-enhanced spin-allowed *d*–*d* transitions in [6]-coordinated Fe^{2+}. The broad, intense, and strongly **E||O**-polarised band at 22000 cm^{-1} is due to Fe^{2+}-Ti^{4+} intervalence charge transfer processes (e.g. Smith, 1978; Taran *et al.*, 1993).

Single-crystal structure refinement

A representative crystal of uvite from Facciatoia was selected for XRD measurements on a Bruker APEX-II single-crystal diffractometer, equipped with a Photon II CCD area detector and a graphite-crystal monochromator, using Mo*K*α radiation from a fine-focus sealed X-ray tube (Dipartimento di Scienze della Terra, University of Pisa). The sample-to-detector distance was 5 cm. A total of 1675 exposures (step = 0.2°, time/step = 20 s) covering a full reciprocal sphere with a redundancy of ~15 was collected using ω and φ scan modes. Final unit-cell parameters were refined using the Bruker AXS *SAINT* program on reflections

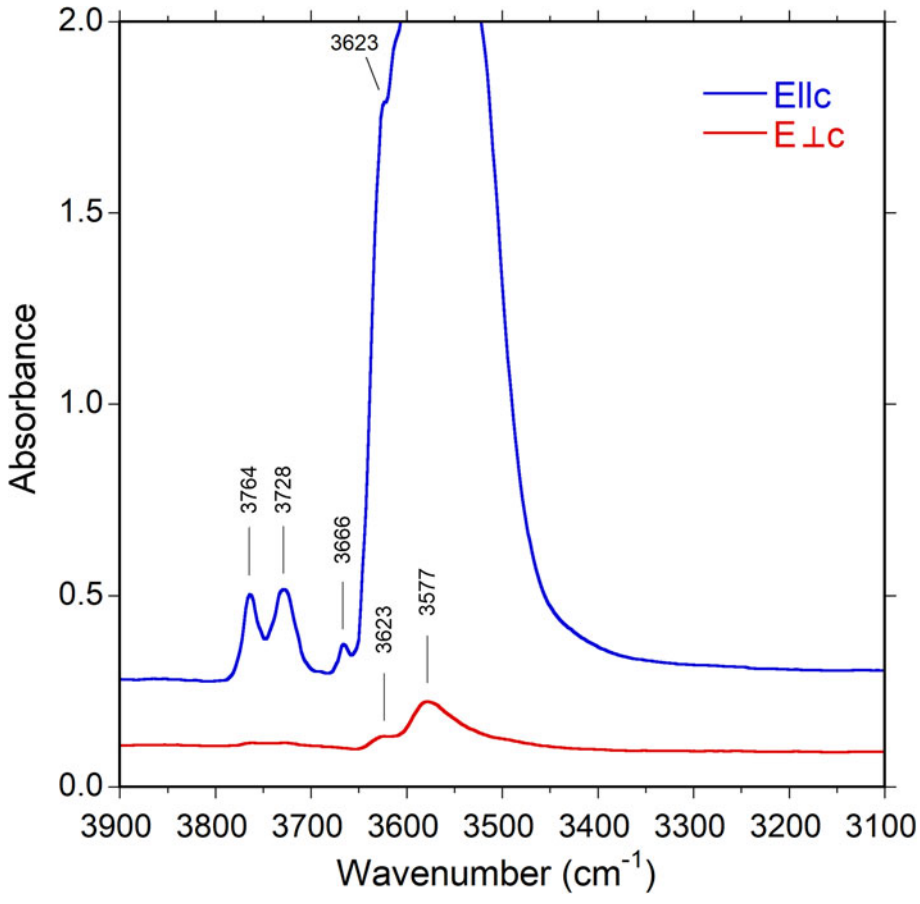

Fig. 3. Polarised FTIR spectra for uvite. Note the presence of bands above 3650 cm^{-1}. The main band is truncated at ~2 absorbance units in the **E||c** direction due to excessive absorption. Sample thickness 39 μm.

https://doi.org/10.1180/mgm.2022.54 Published online by Cambridge University Press

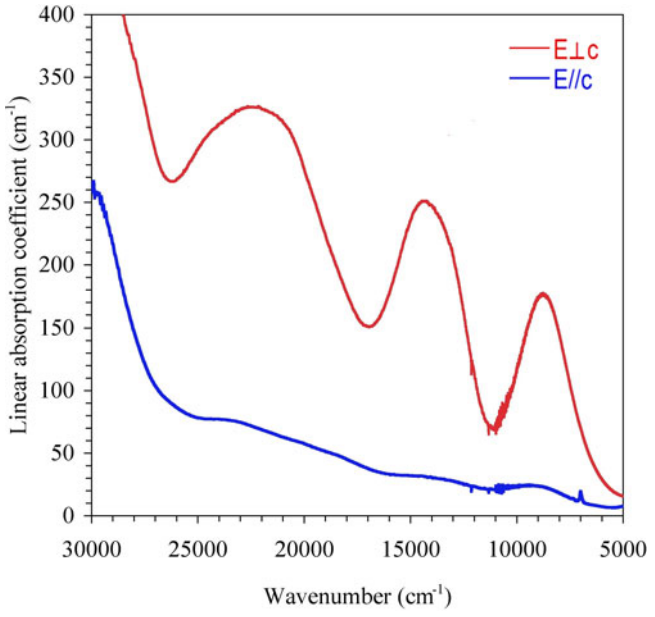

Fig. 4. Polarised optical absorption spectra of uvite in the UV and visible region. Sample thickness 39 μm.

with $I > 10\ \sigma_I$ in the range $5° < 2\theta < 72°$. The intensity data were processed and corrected for Lorentz, polarisation and background effects using the *APEX3* software program of Bruker AXS. The data were corrected for absorption using a multi-scan method (*SADABS*). The absorption correction led to an improvement in R_{int}. No violation of *R*3*m* symmetry was detected.

Structure refinement was done using the *SHELXL-2013* program (Sheldrick, 2015). Starting coordinates were taken from Bosi *et al.* (2017a). Variable parameters were as follows: scale factor, extinction coefficient, atom coordinates, site-scattering values (for *X*, *Y* and *Z* sites) and atomic-displacement factors. Attempts to refine the extinction coefficient yielded values within its standard uncertainty, thus it was not refined. Neutral atom scattering factors were used. In detail, the *X* site was first modelled using Ca *versus* Na, but this yielded a strong correlation ($r = 0.82$) between $^{X}U^{11}$ and the *X* site-scattering value; thus, to avoid this correlation, the *X* site was modelled by setting the Na content to 0.354 atoms per formula unit (apfu, see below) and allowing the remainder of the site to refine as Ca. The occupancy of the *Y* site was obtained considering the presence of Mg *versus* Fe, and the *Z* site with Al *versus* Fe. The *T*, *B* and anion sites were modelled, respectively, with Si, B and O scattering factors and with a fixed occupancy of 1, because refinement with unconstrained occupancies showed no significant deviations from this value. The position of the H(1) and H(3) atoms bonded to oxygen at the O(1) and O(3) sites, respectively, in the structure was taken from the difference-Fourier map and incorporated into the refinement model. In accord with Gatta *et al.* (2014), the O(1)–H(1) and O(3)–H(3) bond lengths were restrained (by DFIX command) to be 0.96 Å and 0.97 Å (respectively) with their isotropic-displacement parameters constrained to be equal to 1.2 times that obtained for the O(1) and O(3) sites. A final refinement was then done by modelling the site occupancy of the O(1) site with O and F fixed at the value obtained from the empirical formula (see below). Similar chemical constraints were applied to refine the H(1) and H(3) sites. There were no correlations greater than 0.7 between the parameters at the end of the refinement. Table 3 lists crystal data, data-collection information, and refinement details; Table 4 gives the fractional atom coordinates, equivalent isotropic-displacement parameters and Table 5 shows selected bond lengths. The crystallographic information file has been deposited with the Principal Editor of *Mineralogical Magazine* and is available as Supplementary material (see below).

Table 3. Single-crystal X-ray diffraction data details for uvite.*

Crystal data	
Crystal size (mm)	0.08 × 0.17 × 0.30
Space-group type	*R*3*m*
a (Å)	15.9519(10)
c	7.2222(5)
V (Å^3)	1591.6(2)
Z	3
Data collection	
Data collection temperature (K)	293
Radiation	Mo*Kα* λ = 0.71073 Å
Axis, frame width (°), time per frame (s)	Phi-omega, 0.2, 20
Range for data collection, 2θ (°)	5–72
Reciprocal space range *hkl*	$-25 \le h \le 25$; $-19 \le k \le 25$; $-11 \le l \le 11$
Set of read reflections	12,296
Unique reflections, R_{int} (%)	1666, 4.37
Unique reflections with $I > 2\sigma(I)$	1664
Redundancy	15
Absorption correction method	Multiscan (*SADABS*)
Refinement	
Refinement method	Full-matrix last-squares on F^2
Structural refinement program	*SHELXL-2013*
Restraints, refined parameters	2, 94
Flack parameter	0.06(3)
wR_2 (%)	4.14
R_1 (%) all data	1.75
R_1 (%) for $I > 2\sigma_I$	1.74
GooF	1.122
Largest diff. hole and peak (e^-/Å^3)	−0.66 and 0.96

*Notes: R_{int} = merging residual value; R_1 = discrepancy index, calculated from *F*-data; wR_2 = weighted discrepancy index, calculated from F^2-data;. Refined as an inversion twin.

Powder X-ray diffraction

A powder X-ray diffraction pattern for uvite was collected at the Natural History Museum of Stockholm (Sweden) using a Panalytical X'pert powder diffractometer equipped with an

Table 4. Fractional atom coordinates, isotropic (*) or equivalent-isotropic displacement parameters (in Å^2) and site occupancies for uvite.

	x/a	*y/b*	*z/c*	$U_{eq/iso}$	Site occupancy
X	0	0	0.22726(15)	0.0152(3)	$Ca_{0.589(6)}Na_{0.354}$
Y	0.12376(4)	0.06188(2)	0.63640(8)	0.00798(16)	$Mg_{0.732(5)}Fe_{0.268(5)}$
Z	0.29823(3)	0.26179(3)	0.61226(7)	0.00624(11)	$Al_{0.982(3)}Fe_{0.018(3)}$
B	0.11005(7)	0.22011(14)	0.4532(3)	0.0073(3)	$B_{1.00}$
T	0.19172(2)	0.19001(2)	0	0.00552(9)	$Si_{1.00}$
O(1) ≡ W	0	0	0.7756(4)	0.0146(5)	$O_{0.945}F_{0.055}$
H(1)	0	0	0.909(4)	0.017*	$H_{0.547}$
O(2)	0.06052(5)	0.12103(11)	0.4791(2)	0.0117(3)	$O_{1.00}$
O(3) ≡ V	0.26505(12)	0.13252(6)	0.5121(2)	0.0130(3)	$O_{1.00}$
H(3)	0.264(2)	0.1321(12)	0.383(3)	0.016*	$H_{1.00}$
O(4)	0.09225(6)	0.18449(11)	0.0717(2)	0.0112(2)	$O_{1.00}$
O(5)	0.18156(11)	0.09078(6)	0.0918(2)	0.0110(2)	$O_{1.00}$
O(6)	0.19536(7)	0.18598(7)	0.77877(15)	0.00934(17)	$O_{1.00}$
O(7)	0.28465(7)	0.28400(7)	0.08006(14)	0.00971(17)	$O_{1.00}$
O(8)	0.20909(7)	0.26967(8)	0.44147(16)	0.01068(18)	$O_{1.00}$

*Isotropic-displacement parameters (U_{iso}) for H(1) and H(3) constrained to have a U_{iso} 1.2 times the U_{eq} value of the O(1) and O(3) oxygen atoms, respectively.

https://doi.org/10.1180/mgm.2022.54 Published online by Cambridge University Press

Table 5. Selected bond lengths (Å) for uvite.

X–O(2) × 3	2.4707(16)	*B*–O(8) × 2	1.3708(14) × 2
X–O(5) × 3	2.6923(16)	*B*–O(2)	1.381(2)
X–O(4) × 3	2.7854(16)	<*B*–O>	1.374
<*X*–O>	2.649		
		T–O(7)	1.5992(10)
Y–O(1)	1.9834(14)	*T*–O(6)	1.6013(11)
Y–O(6) × 2	2.0049(11)	*T*–O(4)	1.6292(6)
Y–O(2) × 2	2.0373(11)	*T*–O(5)	1.6477(7)
Y–O(3)	2.1482(17)	<*T*–O>	1.619
<*Y*–O>	2.036		
Z–O(8)	1.9012(10)		
Z–O(6)	1.9019(11)		
Z–O(7)	1.9110(10)		
Z–O(8)'	1.9334(11)		
Z–O(7)'	1.9669(11)		
Z–O(3)	1.9909(8)		
<*Z*–O>	1.934		

X'celerator silicon-strip detector. The range 5–80° (2θ) was scanned with a step-size of 0.017° with the sample mounted on a background-free Si holder using sample spinning. The diffraction data (for Cu*K*α = 1.54059 Å), corrected using Si as an internal standard, are listed in Table 6. The program *UnitCell* (Holland and Redfern, 1997) was used to refine unit-cell parameters in the trigonal system: $a = 15.9729(3)$ Å, $c = 7.2291(2)$ Å and $V = 1597.3(1)$ Å^3.

Table 6. Powder X-ray diffraction data for uvite.*

h	*k*	*l*	*I* (%)	d_{meas} (Å)	d_{cal} (Å)
1	0	1	16	6.409	6.407
0	2	1	16	4.997	4.998
0	3	0	14	4.611	4.611
2	**1**	**1**	**49**	**4.237**	**4.236**
2	**2**	**0**	**51**	**3.994**	**3.993**
0	**1**	**2**	**57**	**3.497**	**3.497**
1	3	1	11	3.389	3.389
1	4	0	14	3.019	3.019
1	**2**	**2**	**88**	**2.973**	**2.973**
3	2	1	9	2.906	2.906
3	1	2	8	2.631	2.631
0	**5**	**1**	**100**	**2.584**	**2.584**
0	0	3	15	2.409	2.410
2	3	2	17	2.385	2.385
5	1	1	16	2.349	2.350
5	0	2	12	2.197	2.197
4	3	1	16	2.169	2.169
3	0	3	11	2.135	2.136
4	2	2	8	2.118	2.118
2	2	3	20	2.063	2.063
1	**5**	**2**	**53**	**2.047**	**2.047**
1	6	1	5	2.025	2.025
4	4	0	5	1.996	1.997
3	4	2	37	1.925	1.925
1	4	3	7	1.883	1.883
6	2	1	9	1.854	1.854
3	3	3	7	1.786	1.787
0	6	3	26	1.666	1.666
2	7	1	18	1.645	1.646
5	5	0	25	1.597	1.597
0	9	0	5	1.537	1.537
7	2	2	6	1.531	1.531
0	5	4	19	1.513	1.513
5	1	4	21	1.461	1.462
0	1	5	5	1.438	1.438
6	5	1	9	1.422	1.422
4	3	4	15	1.415	1.415
0	11	1	5	1.239	1.239

*Only the reflections with $I \geq 5\%$ are listed. The six strongest reflections are given in bold.

Table 7. Refined site-scattering values and optimised site-populations for uvite.

Site	Refined site-scattering (epfu[a])	Optimised site-population (apfu[b])	Calculated site-scattering (epfu)
X	15.69(9)	0.61 Ca + 0.35 Na + 0.04 □	16.10
Y	47.26(24)	1.50 Mg + 0.47 Fe^{2+} + 0.71 Al + 0.14 Fe^{3+} + 0.18 Ti	47.04
Z	79.40(24)	4.54 Al + 0.18 Fe^{3+} + 0.02 V^{3+} + 1.27 Mg	79.19

[a] = electrons per formula unit; [b] = atoms per formula unit

Determination of the number of atoms per formula unit

In agreement with the structure-refinement results, the boron content was assumed to be stoichiometric ($B^{3+} = 3.00$ apfu). Both the site-scattering results and the bond lengths of *B* and *T* are consistent with the *B* site fully occupied by boron and no amount of B^{3+} at the *T* site (e.g. Bosi and Lucchesi, 2007). The iron oxidation state was determined by MS. In accordance with Pesquera *et al.* (2016), the Li content was assumed to be insignificant as MgO > 2 wt.% in the sample studied. The (OH) content and the formula were then calculated by charge balance with the assumption (T + Y + Z) = 15 apfu and 31 anions pfu (Table 1). The excellent agreement between the number of electrons per formula unit (epfu) derived from EMPA and SREF (241.2 and 241.1 epfu, respectively) supports the stoichiometric assumptions.

Site populations

The uvite site populations at the *X*, *B*, *T*, O(3) (≡ V) and O(1) (≡ W) sites follow the standard site preference suggested for tourmaline (e.g. Henry *et al.*, 2011) and are in accord with the information from FTIR absorption spectra (Fig. 3). The site populations at the octahedrally coordinated *Y* and *Z* sites were optimised according to the procedure of Bosi *et al.* (2017b), and by fixing the minor elements Ti^{4+} at *Y* and V^{3+} at *Z*.

The resulting empirical crystal-chemical formula is:

$$^{X}(Ca_{0.61}Na_{0.35}\square_{0.04})_{\Sigma 1.00}\,^{Y}(Mg_{1.50}Fe^{2+}_{0.47}Al_{0.71}Fe^{3+}_{0.14}Ti_{0.18})_{\Sigma 3.00}$$
$$^{Z}(Al_{4.54}Fe^{3+}_{0.18}V^{3+}_{0.02}Mg_{1.27})_{\Sigma 6.00}\,^{T}[(Si_{5.90}Al_{0.10})_{\Sigma 6.00}O_{18}]$$
$$(BO_3)_3\,^{O(3)}(OH)_3\,^{O(1)}[(OH)_{0.55}F_{0.05}O_{0.40}]_{\Sigma 1.00}$$

The refined site-scattering values (Hawthorne *et al.*, 1995) and those calculated from the site populations are compared in Table 7. The agreement between the refined and calculated values is very good, and validates the distribution of cations over the *X*, *Y* and *Z* sites. These site populations are also supported by the close accord of the weighted bond-valence sums and weighted atom valences (or mean formal charges) calculated from the empirical crystal-chemical formula (Table 8).

For classification purposes, the optimised formula was recast in its ordered form, i.e. with trivalent cations ordered in the Z position of the tourmaline general chemical formula (Henry *et al.*, 2011):

https://doi.org/10.1180/mgm.2022.54 Published online by Cambridge University Press

Table 8. Weighted bond-valences (valence units) for uvite.*

Site	*X*	*Y*	*Z*	*T*	*B*	Σ_{anion}
O(1)		$0.44^{\times 3\rightarrow}$				1.32
O(2)	$0.21^{\times 3\downarrow}$	$0.39^{\times 2\downarrow\rightarrow}$			0.97	1.97
O(3)		0.30	$0.4^{\times 2\rightarrow}$			1.12
O(4)	$0.10^{\times 3\downarrow}$			$0.99^{\times 2\rightarrow}$		2.07
O(5)	$0.12^{\times 3\downarrow}$			$0.94^{\times 2\rightarrow}$		2.00
O(6)		$0.43^{\times 2\downarrow}$	0.51	1.06		2.00
O(7)			0.50	1.07		2.00
			0.43			
O(8)			0.47		$1.00^{\times 2\downarrow}$	1.99
			0.51			
Σ_{cation}	1.29	2.39	2.84	4.06	2.98	
MFC[a]	1.57	2.40	2.79	3.98	3.00	

*Notes: Weighted bond valence according to Bosi (2014); bond valence parameters from Gagné and Hawthorne (2015).
[a]Mean Formal Charge (or weighted atom valence) from the empirical crystal-chemical formula.

$$^{X}(Ca_{0.61}Na_{0.35}\square_{0.04})_{\Sigma 1.00}\ ^{Y}(Mg_{2.35}Fe^{2+}_{0.47}Ti_{0.18})_{\Sigma 3.00}$$
$$^{Z}(Al_{5.25}Fe^{3+}_{0.32}V^{3+}_{0.02}Mg_{0.42})_{\Sigma 6.00}\ ^{T}[(Si_{5.90}Al_{0.10})_{\Sigma 6.00}O_{18}]$$
$$(BO_3)_3\ ^{V}(OH)_3\ ^{W}[(OH)_{0.55}F_{0.05}O_{0.40}]_{\Sigma 1.00}$$

End-member formula and relation to other species

The composition of the sample is consistent with a hydroxy-tourmaline belonging to the calcic group (Henry *et al.*, 2011): it is Ca-dominant at the X position of the tourmaline general formula and hydroxy-dominant at W with $(OH)^- > O^{2-}$. As divalent-cations (with Mg) are the dominant Y-constituent, formula electroneutrality requires a Z-total charge = +17 in the end-member formula: $CaMg_3(Z_6)^{\Sigma 17+}(Si_6O_{18})(BO_3)_3(OH)_3(OH)$. The unique charge arrangement compatible with the Z-constituents is $^{Z}(3^{+}_{5}2^{+})$, which correspond to the atomic arrangement $^{Z}(Al^{3+}_{5}Mg^{2+})$. Therefore, the uvite end-member formula is $CaMg_3(Al_5Mg)(Si_6O_{18})(BO_3)_3(OH)_3(OH)$. As no tourmalines are currently approved with this composition, it can be classified as a new species.

Uvite is related to fluor-uvite, ideally $CaMg_3(Al_5Mg)(Si_6O_{18})(BO_3)_3(OH)_3F$, and feruvite, ideally $CaFe^{2+}_3(Al_5Mg)(Si_6O_{18})(BO_3)_3(OH)_3(OH)$, by the homovalent substitutions $^{W}(OH)^- \leftrightarrow {}^{W}F^-$ and $^{Y}Mg^{2+} \leftrightarrow {}^{Y}Fe^{2+}$, respectively. Uvite is also related to magnesio-lucchesiite by the heterovalent substitution $^{Z}Mg^{2+} + {}^{W}(OH)^- \leftrightarrow {}^{Z}Al^{3+} + {}^{W}O^{2-}$. The properties of these four tourmalines are compared in Table 9.

Calcic tourmalines from the thermal aureole of the Monte Capanne intrusion at San Piero in Campo: historical background and genetic inferences

To date, eleven tourmaline species have been identified from Elba Island. The origin of these tourmalines is both pegmatitic (elbaite, fluor-elbaite, schorl, foitite, rossmanite, tsilaisite, fluor-tsilaisite and celleriite) and non-pegmatitic related to basic hornfels which are mostly meta-serpentinites more or less altered by late-stage fluids (Ca-rich dravite, magnesio-lucchesiite and uvite) (e.g. Dini and Pezzotta, 2021). Among them, elbaite (Vernadsky, 1914), tsilaisite (Bosi *et al.*, 2012), fluor-tsilaisite (Bosi *et al.*, 2015b), magnesio-lucchesiite (Scribner *et al.*, 2021), celleriite (Bosi *et al.*, 2022) and uvite (this study) have Elba Island as type locality. Uvite is the second calcic tourmaline, after magnesio-lucchesiite, discovered in the San Piero in Campo

Table 9. Comparative data for uvite, fluor-uvite, magnesio-lucchesiite and feruvite.*

	Uvite	Fluor-uvite	Magnesio-lucchesiite	Feruvite
Formula	$CaMg_3(Al_5Mg)(Si_6O_{18})(BO_3)_3(OH)_3(OH)$	$CaMg_3(Al_5Mg)(Si_6O_{18})(BO_3)_3(OH)_3F$	$CaMg_3(Al_6)(Si_6O_{18})(BO_3)_3(OH)_3O$	$CaFe^{2+}_3(Al_5Mg)(Si_6O_{18})(BO_3)_3(OH)_3(OH)$
a (Å)	15.951(1)	15.954(1)	15.9910(3)	16.012(2)
c	7.2222(5)	7.214(1)	7.2224(2)	7.245(2)
V (Å^3)	1591.6(2)	1590.2(3)	1599.42(7)	1606.6(4)
Space-group type	*R3m*	*R3m*	*R3m*	*R3m*
Optic sign	Uniaxial (–)	Uniaxial (–)	Uniaxial (–)	Uniaxial (–)
ω	1.660(5)	1.637-1.668	1.668	1.687(1)
ε	1.640(5)	1.619-1.639	1.644	1.669(1)
Streak	Grey	Black, greenish-black, brownish-black, brown, green, colourless	–	Grey
Colour	Brown	Light-brown, light-green or white	Brown	Dark brown-black
Pleochroism	O = greenish brown E = pale yellow	O = pale yellow E = colourless	O = dark brown E = colourless to dark brown	O = light brown E = very dark brown
Strongest lines in the powder XRD pattern *d*(Å) (*I*, %)	2.584 (100) 2.973 (88) 3.497 (57) 2.047 (53) 3.994 (51) 4.24 (49)	2.62 (100) 3.35 (82) 10.0 (73) 3.15 (64) 3.39 (58) 1.536 (52) 2.43 (48) 2.65 (41)	2.59 (100) 2.97 (70) 4.00 (58) 4.24 (54) 3.49 (46) 2.05 (46) 6.40 (32)	2.586 (100) 2.979 (80) 4.24 (60) 4.00 (60) 3.50 (60) 2.051 (50) 6.43 (40)
Reference	This work	Mindat.org; Dunn *et al.* (1977)	Scribner *et al.* (2019)	Grice and Robinson (1989)

*Notes: The pleochroism reported in Grice and Robinson (1989) is anomalous. All other tourmalines reported so far in literature display a reverse pleochroic scheme with O > E.

https://doi.org/10.1180/mgm.2022.54 Published online by Cambridge University Press

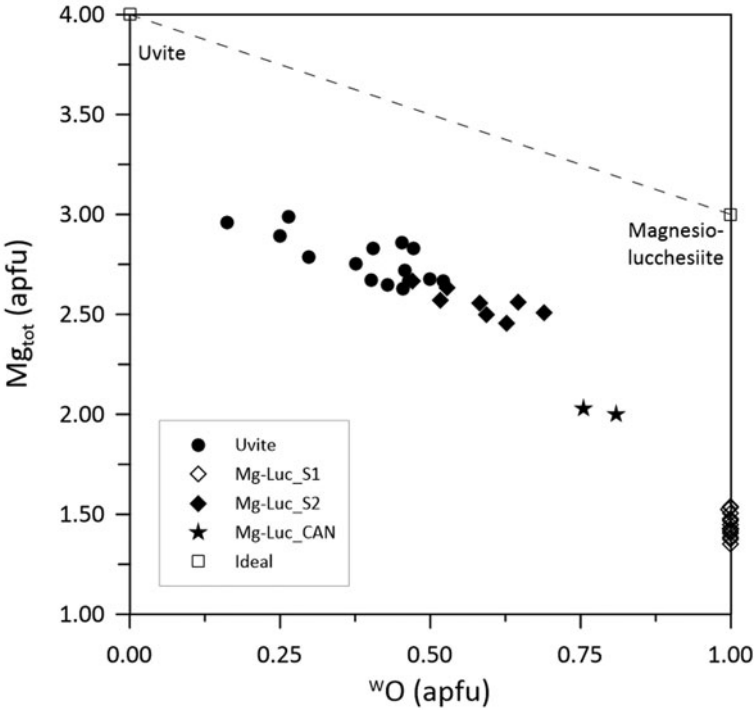

Fig. 5. The plot of Mg_{tot} *versus* $^{W}O^{2-}$ showing the occurrence of a solid-solution between uvite and magnesio-lucchesiite according to the substitution $^{Z}Mg^{2+} + {}^{W}(OH)^{-} \leftrightarrow {}^{Z}Al^{3+} + {}^{W}O^{2-}$ (see text). Data are single spot analyses of the uvite sample from this study (spots = 15) and magnesio-lucchesiite samples from Scribner *et al.* (2021) (Samples S1 and S2 from Elba Island, spots = 16 and 7, respectively; sample CAN from Canada, spots = 2).

area. This locality has been well known since the late 18th Century for the occurrence of multi-coloured tourmaline specimens related to the presence of gem-bearing pegmatites (Pezzotta, 2021). The presence of black tourmaline in metabasite from Elba Island has been known since the 1820s (e.g. Soret, 1822) and further descriptions were given by vom Rath (1870), D'Achiardi (1873), Viola and Ferrari (1911) and Millosevich (1914).

In metabasite from San Piero in Campo, calcic tourmalines (uvite and magnesio-lucchesiite) occur in the southeastern sector of the area, where metaserpentinite is in contact with intrusive rocks and are characterised by small vein systems filled by black-to-brown tourmalines. Veins are up to 2–3 cm thick and up to 1 m long. Their origin may be related to the influx of B-rich fluids released by the nearby pegmatite veins or leucogranitic and aplitic bodies during their crystallisation. The interaction between these B-rich fluids and (Ca/Mg)-rich metaserpentinites is consistent with the genesis of (Ca/Mg)-rich tourmalines. The compositions and the nature of the country rocks seem to control the crystal-chemistry of the calcic tourmalines from San Piero in Campo. Indeed, uvite has been identified in veins from the Facciatoia locality, hosted in deeply hydrothermalised metaserpentinite crosscut by magnesite + dolomite veins, nearby an LCT-pegmatite and a lens of Santa'Andrea facies monzogranite (Farina *et al.*, 2010).

In the same area, magnesio-lucchesiite was identified by Scribner *et al.* (2021) in veins along fractures of a spinel-bearing rock occurring some hundreds of metres south-west of Facciatoia (San Rocco locality). Such veins contain tourmaline extremely enriched in Al (~7.7 apfu) with the spinel phase corresponding to Fe-bearing spinel, $(Mg_{0.7}Fe^{2+}_{0.3})_{\Sigma 1.0}(Al_{1.9}Fe^{3+}_{0.1})_{\Sigma 2.0}O_4$, as determined by energy dispersive spectroscopy analyses. Scribner *et al.* (2021) identified in San Rocco a second occurrence of a solid solution between magnesio-lucchesiite and uvite relatively depleted in Al (~5.6 apfu), in veins along fractures within a basic hornfels derived by contact metamorphism of serpentinite.

The plot of Mg_{tot} *versus* $^{W}O^{2-}$ of the single spot analyses of the present uvite and the above-mentioned magnesio-lucchesiite samples show the occurrence of a solid-solution between these minerals (Fig. 5). The negative relation between Mg_{tot} and $^{W}O^{2-}$ is consistent in the substitution mechanism $^{Z}Mg^{2+} + {}^{W}(OH)^{-} \leftrightarrow {}^{Z}Al^{3+} + {}^{W}O^{2-}$. Note that Mg_{tot} was preferred to ^{Z}Mg in Fig. 5 to remove issues of uncertainty associated with Mg and Al order–disorder over the *Y* and *Z* sites. In conclusion, the solid-solution between uvite and magnesio-lucchesiite is documented and shows the extreme sensitivity of the tourmaline-supergroup minerals to record subtle geochemical changes in the environment of crystallisation.

Environments of uvite formation

High Ca and low F and Al contents are essential for stabilisation of uvite in contrast to other tourmaline species such as dravite, fluor-uvite and magnesio-lucchesiite. These specific conditions therefore require both specific host lithology and fluid composition.

Uvite occurrence in mafic rocks, similar to the type locality, was noted by Scribner *et al.* (2018) who described uvite associated with Fe-rich dravite and Mg- and Ti-rich feruvite (and magnesio-lucchesiite; Scribner *et al.*, 2021) in metasomatically altered lamprophyre dykes. The tourmaline formed by replacement of magmatic Ca-amphibole (actinolite to magnesio-hornblende) and its specific composition was constrained by the high Ca and low Al contents in the system during the metasomatic reaction.

Although tourmaline from calc-dolomite marbles is commonly described as 'uvite', these tourmalines typically contain high F and/or Na contents resulting in formation of fluor-uvite–magnesio-lucchesiite or dravite–oxy-dravite–magnesio-foitite solid solutions (e.g. Bačík *et al.*, 2012; Krmíček *et al.*, 2021; Dutrow and Henry, 2021). The occurrence of uvite with fluor-uvite in pockets of Portage-du-Fort marble, Québec, Canada, is a notable exception (Belley *et al.*, 2014); uvite with significant ^{W}O contents

https://doi.org/10.1180/mgm.2022.54 Published online by Cambridge University Press

(*ca.* 0.3–0.45 apfu; recalculation of original data to electroneutral formulae) forms mainly as a late retrograde mineral replacing serendibite in generations 5 and 6 in Belley *et al.* (2014). Its association with fluor-uvite and fluor-dravite (generation 4) indicates that it formed from a F- and Na-depleted fluid at the final stages of retrograde tourmaline crystallisation.

In addition to specific Ca- and Mg-rich, Al-depleted environments such as hydrothermal veins in metaserpentinites (type locality) or metasomatically altered lamprophyres (Scribner *et al.*, 2018), uvite may also form the fluor-uvite assemblages as a result of gradual change of fluid composition or local fluctuation in F content. The different environments and conditions that favour crystallisation of uvite show that calcic tourmalines may serve as an effective petrogenetic probe for monitoring fluid composition in hydrothermal and metamorphic systems.

Acknowledgments. Chemical analyses were done with the kind assistance of M. Serracino to whom the authors express their gratitude. F.B. acknowledges funding by Sapienza University of Rome (Prog. Università 2020). C.B. and F.B. acknowledges funding by the Ministero dell'Università e della Ricerca through the project PRIN 2020 "HYDROX – HYDRous- vs OXo-components in minerals: adding new pieces to the Earth's H_2O cycle puzzle", prot. 2020WYL4NY. F.C.H. acknowledges a Discovery Grant from the Natural Sciences and Engineering Council of Canada. Comments by the Structural Editor (P. Leverett) and reviewers (Vincent van Hinsberg and Oleg Vereshchagin) are very much appreciated.

Supplementary material. To view supplementary material for this article, please visit https://doi.org/10.1180/mgm.2022.54

Competing interests. The authors declare none.

References

Bačík P. and Fridrichová G. (2021) Cation partitioning among crystallographic sites based on bond-length constraints in tourmaline-supergroup minerals. *American Mineralogist*, **106**, 851–861.

Bačík P., Uher P., Cempírek J. and Vaculovič T. (2012) Magnesian tourmalines from plagioclase–muscovite–scapolite metaevaporite layers in dolomite marble near Prosetín (Olešnice Unit, Moravicum, Czech Republic). *Journal of Geosciences*, **57**, 143–153.

Belley P.M., Grice J.D., Fayek M., Kowalski P.M. and Grew E.S. (2014) A new occurrence of the borosilicate serendibite in tourmaline-bearing calc-silicate rocks, Portage-du-Fort marble, Grenville Province, Québec: evolution of boron isotope and tourmaline compositions in a metamorphic context. *The Canadian Mineralogist*, **52**, 595–616.

Berryman E.J., Wunder B., Ertl A., Koch-Müller M., Rhede D., Scheidl K., Giester G. and Heinrich W. (2016) Influence of the *X*-site composition on tourmaline's crystal structure: Investigation of synthetic K-dravite, dravite, oxy-uvite, and magnesio-foitite using SREF and Raman spectroscopy. *Physics and Chemistry of Minerals*, **43**, 83–102.

Bosi F. (2013) Bond-valence constraints around the O1 site of tourmaline. *Mineralogical Magazine*, **77**, 343–351.

Bosi F. (2014) Bond valence at mixed occupancy sites. I. Regular polyhedra. *Acta Crystallographica*, **B70**, 864–870.

Bosi F. (2018) Tourmaline crystal chemistry. *American Mineralogist*, **103**, 298–306.

Bosi F. and Lucchesi S. (2007) Crystal chemical relationships in the tourmaline group: structural constraints on chemical variability. *American Mineralogist*, **92**, 1054–1063.

Bosi F., Skogby H., Agrosì G. and Scandale E. (2012) Tsilaisite, $NaMn_3Al_6(Si_6O_{18})(BO_3)_3(OH)_3OH$, a new mineral species of the tourmaline supergroup from Grotta d'Oggi, San Pietro in Campo, island of Elba, Italy. *American Mineralogist*, **97**, 989–994.

Bosi F., Skogby H., Lazor P. and Reznitskii L. (2015a) Atomic arrangements around the O3 site in Al- and Cr-rich oxy-tourmalines: a combined EMP, SREF, FTIR and Raman study. *Physics and Chemistry of Minerals*, **42**, 441–453.

Bosi F., Andreozzi G.B., Agrosì G. and Scandale E. (2015b) Fluor-tsilaisite, $NaMn_3Al_6(Si_6O_{18})(BO_3)_3(OH)_3F$, a new tourmaline from San Piero in Campo (Elba, Italy) and new data on tsilaisitic tourmaline from the holotype specimen locality. *Mineralogical Magazine*, **79**, 89–101.

Bosi F., Skogby H., Ciriotti M.E., Gadas P., Novák M., Cempírek J., Všianský D. and Filip J. (2017a) Lucchesiite, $CaFe^{2+}_3Al_6(Si_6O_{18})(BO_3)_3(OH)_3O$, a new mineral species of the tourmaline supergroup. *Mineralogical Magazine*, **81**, 1–14.

Bosi F., Reznitskii L., Hålenius U. and Skogby H. (2017b) Crystal chemistry of Al–V–Cr oxy-tourmalines from Sludyanka complex, Lake Baikal, Russia. *European Journal of Mineralogy*, **29**, 457–472.

Bosi F., Skogby H., Hålenius U. and Ciriotti M. (2018) Experimental cation redistribution in the tourmaline lucchesiite, $CaFe^{2+}_3Al_6(Si_6O_{18})(BO_3)_3(OH)_3O$. *Physics and Chemistry of Minerals*, **45**, 621–632.

Bosi F., Biagioni C., Pezzotta F., Skobgy H., Hålenius U., Cempírek J., Hawthorne F.C., Lussier A.J., Abdu Y.A., Day M.C., Fayek M., Clark C.M., Grice J.D. and Henry D.J. (2020) Uvite, IMA 2019-113; CNMNC Newsletter 54. *European Journal of Mineralogy*, 32, https://doi.org/10.5194/ejm-32-275-2020.

Bosi F., Pezzotta F., Altieri A., Andreozzi G.B., Ballirano P., Tempesta G., Cempírek J., Škoda R., Filip J., Čopjaková R., Novák M., Kampf A.R., Scribner E.D., Groat L.A. and Evans R.J. (2022) Celleriite, $\square(Mn^{2+}_2Al)Al_6(Si_6O_{18})(BO_3)_3(OH)_3(OH)$, a new mineral species of the tourmaline supergroup. *American Mineralogist*, **107**, 31–42.

Cempírek J., Houzar S., Novák M., Groat L.A., Selway J.B. and Šrein V. (2013) Crystal structure and compositional evolution of vanadium-rich oxy-dravite from graphite quartzite at Bítovánky, Czech Republic. *Journal of Geosciences*, **58**, 149–162.

Clark C.M., Hawthorne F.C. and Grice J.D. (2010) Uvite, IMA 2000-030a. CNMNC Newsletter, April 2010, page 377. *Mineralogical Magazine*, **74**, 375–377.

D'Achiardi A. (1873) *Mineralogia della Toscana*. Vol. II. Tipografia Nistri, Pisa, Italy, 404 pp.

Dini A. and Pezzotta F. (2021) Tourmalines from Elba Island: geology and genesis. *Rivista Mineralogica Italiana*, **45**, 146–153.

Dunn P.J., Appleman D., Nelen J. and Norberg J. (1977) Uvite, a new (old) common member of the tourmaline group and its implications for collections. *Mineralogical Record*, **8**, 100–108.

Dutrow B.L. and Henry D.J. (2021) Petrogenetic utility of magnesian tourmaline: extraordinary origin of everyday tourmaline. *NATURA*, **111**, 29–30.

Ertl A., Hughes J.M., Pertlik F., Foit F.F. Jr., Wright S.E., Brandstatter F. and Marler B. (2002) Polyhedron distortions in tourmaline. *The Canadian Mineralogist*, **40**, 153–162.

Farina F., Dini A., Innocenti F., Rocchi S. and Westerman D.S. (2010) Rapid incremental assembly of the Monte Capanne pluton (Elba Island, Tuscany) by downward stacking of magma sheets. *Geological Society of America Bulletin*, **122**, 1463–1479.

Foit F.F. Jr. (1989) Crystal chemistry of alkali-deficient schorl and tourmaline structural relationships. *American Mineralogist*, **74**, 422–431.

Gagné O.C. and Hawthorne F.C. (2015) Comprehensive derivation of bond-valence parameters for ion pairs involving oxygen. *Acta Crystallographica*, **B71**, 562–578.

Gatta G.D., Bosi F., McIntyre G.J. and Skogby H. (2014) First accurate location of two proton sites in tourmaline: A single-crystal neutron diffraction study of oxy-dravite. *Mineralogical Magazine*, **78**, 681–692.

Gonzales-Carreño T., Fernández M. and Sanz J. (1988) Infrared and electron microprobe analysis of tourmaline. *Physics and Chemistry of Minerals*, **15**, 452–460.

Grice J.D. and Robinson G.W. (1989) Feruvite, a new member of the tourmaline group, and its crystal structure. *The Canadian Mineralogist*, **27**, 199–203.

Hålenius U., Hatert F., Pasero M. and Mills S.J. (2018) New minerals and nomenclature modifications approved in 2017 and 2018 (IMA-CNMNC Newsletter 41). *Mineralogical Magazine*, **82**, 229–233.

Hawthorne F.C. (1996) Structural mechanisms for light-element variations in tourmaline. *The Canadian Mineralogist*, **34**, 123–132.

Hawthorne F.C. and Henry D. (1999) Classification of the minerals of the tourmaline group. *European Journal of Mineralogy*, **11**, 201–215.

Hawthorne F.C., Ungaretti L. and Oberti R. (1995) Site populations in minerals: terminology and presentation of results of crystal-structure refinement. *The Canadian Mineralogist*, **33**, 907–911.

Henry D.J. and Dutrow B.L. (2011) The incorporation of fluorine in tourmaline: Internal crystallographic controls or external environmental influences? *The Canadian Mineralogist*, **49**, 41–56.

Henry D.J., Novák M., Hawthorne F.C., Ertl A., Dutrow B., Uher P. and Pezzotta F. (2011) Nomenclature of the tourmaline supergroup minerals. *American Mineralogist*, **96**, 895–913.

Holland T.J.B. and Redfern S.A.T. (1997) Unit cell refinement from powder diffraction data: the use of regression diagnostics. *Mineralogical Magazine*, **61**, 65–77.

Krmíček L., Novák M., Trumbull R.B., Cempírek J. and Houzar S. (2021) Boron isotopic variations in tourmaline from metacarbonates and associated calc-silicate rocks from the Bohemian Massif: A first study constraints on boron recycling in the Variscan orogen. *Geoscience Frontiers*, **12**, 219–230.

Kunitz W. (1929) Die Mischungsreihen in der Turmalingruppe und die genetischen Beziehungen zwischen Turmalinen und Glimmern. *Chemie der Erde*, **4**, 208–251.

Mandarino J.A. (1981) The Gladstone-Dale relationship. Part IV: the compatibility concept and its application. *The Canadian Mineralogist*, **19**, 441–450.

Mattson S.M and Rossman G.R. (1987) Fe^{2+}-Fe^{3+} interactions in tourmaline. *Physics and Chemistry of Minerals*, **14**, 163–171.

Millosevich F. (1914) *I 5000 elbani del Museo di Firenze*. Studio Editoriale Insubria, Reprint Milano, 1978, 96 p. [in Italian].

Novák M., Povondra P. and Selway J.B. (2004) Schorl-oxy-schorl to dravite-oxydravite tourmaline from granitic pegmatites; examples from the Moldanubicum, Czech Republic. *European Journal of Mineralogy*, **16**, 323–333.

Pesquera A., Gil-Crespo P.P, Torres-Ruiz F., Torres-Ruiz J. and Roda-Robles E. (2016) A multiple regression method for estimating Li in tourmaline from electron microprobe analyses. *Mineralogical Magazine*, **80**, 1129–1133.

Pezzotta F. (2021) A history of tourmaline from the Island of Elba. *The Mineralogical Record*, **52**, 669–720.

Pouchou J.L. and Pichoir F. (1991) Quantitative analysis of homogeneous or stratified microvolumes applying the model "PAP." Pp. 31–75 in: *Electron Probe Quantitation* (K.F.J. Heinrich and D.E. Newbury, editors). Plenum, New York.

Prescher C., McCammon C. and Dubrowinsky L. (2012) *MossA*: a program for analyzing energy-domain Mössbauer spectra from conventional and synchrotron sources. *Journal of Applied Crystallography*, **45**, 329–331.

Rath G. (1870) Geognostich-mineralogische Fragmente aus Italien. III. Theil. Die Insel Elba. *Zeitschrift der Deutschen Geologischen Gesellschaft*, **22**, 591–731.

Scribner E.D., Groat L.A. and Cempírek J. (2018) Mineralogy of Ti-bearing, Al-deficient tourmaline assemblages associated with lamprophyre dikes near the O'Grady Batholith, Northwest Territories, Canada. *Journal of Geosciences*, **63**, 123–135.

Scribner E.D., Cempírek J., Groat L.A., Evans R.J., Biagioni C., Bosi F., Dini A, Hålenius U., Orlandi P. and Pasero M. (2021) Magnesio-lucchesiite, $CaMg_3Al_6(Si_6O_{18})(BO_3)_3(OH)_3O$, a new species of the tourmaline supergroup. *American Mineralogist*, **106**, 862–871.

Sheldrick G.M. (2015) Crystal structure refinement with SHELXL. *Acta Crystallographica*, **C71**, 3–8.

Smith G. (1978) A reassessment of the role of iron in the 5,000 - 30,000 cm^{-1} region of the electronic absorption spectra of tourmaline. *Physics and Chemistry of Minerals*, **3**, 343–373.

Soret F. (1822) Sur les minéraux rares ou offrant des cristallisations nouvelles, observes dans la collection du Musée Académique du Genève. *Mémoires de la Société de physique et d'histoire naturelle de Genève*, **1**, 465–499.

Taran M.N., Lebedev A.S. and Platonov A.N. (1993) Optical absorption spectroscopy of synthetic tourmalines. *Physics and Chemistry of Minerals*, **20**, 209–220.

Vernadsky W. (1914) XXII. Über die chemische Formel der Turmaline. *Zeitschrift für Kristallographie – Crystalline Materials*, **53**, 273–288 [in German].

Viola C. and Ferrari M. (1911) Rocce a pleonasto di S. Piero in Campo Elba. *Atti della R. Accademia dei Lincei, Memorie*, **308**, 429–436.

Watenphul A., Burgdorf M., Schlüter J., Horn I., Malcherek T. and Mihailova B. (2016) Exploring the potential of Raman spectroscopy for crystallochemical analyses of complex hydrous silicates: II. Tourmalines. *American Mineralogist*, **101**, 970–985.

https://doi.org/10.1180/mgm.2022.54 Published online by Cambridge University Press